 doi:10.20944/preprints202110.0411.v1

Type of the Paper (Article, Review, Communication, etc.)

Investigation of the extrapolation capability of an Artificial Neural Network Algorithm in combination with Process Signals in Resistance Spot Welding of Advanced High-Strength Steels

Bassel El-Sari [1]*, Max Biegler [1] and Michael Rethmeier [2, 1,3]

[1] Fraunhofer IPK, Pascalstr. 8-9, 10587 Berlin Germany; bassel.el-sari@ipk.fraunhofer.de; max.biegler@ipk.fraunhofer.de; michael.rethmeier@ipk.fraunhofer.de
[2] Technische Universität Berlin, Chair of Joining, Straße des 17. Juni 135, 10623 Berlin Germany
[3] Bundesanstalt für Materialforschung und -prüfung (BAM), Unter den Eichen 87, 12205 Berlin Germany
* Correspondence: bassel.el-sari@ipk.fraunhofer.de; Tel.: +49 (0) 30-39006-295

Abstract: Resistance spot welding is an established joining process in the production of safety-relevant components in the automotive industry. Therefore, a consecutive process monitoring is essential to meet the high-quality requirements. Artificial neural networks can be used to evaluate the process parameters and signals to ensure the individual spot weld quality. The predictive accuracy of such algorithms depends on the provided training data set and the prediction of untrained data is challenging. The aim of this paper is to investigate the extrapolation capability of the multi-layer perceptron model. That means, that the predictive performance of the model will be tested with data that clearly differs from the training data in terms of material and coating composition. Therefore, three multi-layer perceptron regression models were implemented to predict the nugget diameter from process data. The three models were able to predict the trained datasets very well. The models, which were provided with features from the dynamic resistance curve predicted the new dataset better than the model with only process parameters. This study shows the beneficial influence of the process signals on the predictive accuracy and robustness of artificial neural network algorithms. Especially, when predicting a data set from outside of the training space.

Keywords: Automotive; Resistance Spot Welding; Quality Assurance; Quality Monitoring; Artificial Intelligence

1. Introduction

Resistance spot welding (RSW) is an efficient and highly automated joining technology used in the car manufacturing. A typical car body has up to 5000 resistance spot welds [1] with a varying number of joining partners, different materials and different sheet thicknesses [2]. These variations, the high process speed and the several sources of errors, like gaps and improper component alignment [3] increase the process complexity [4]. This is also reflected in the high testing efforts and the extensive destructive tests in mass production [3]. An automotive production line of high-volume models produces daily more than 7 million welds [5]. It can be estimated that up to 20% of the spot welds are only made to ensure the component safety of welded assemblies [6]. Hence, a reliable process monitoring is essential to save costs and limit the production effort.

The welding power supply manufacturer developed real-time control approaches [7] that record the dynamic resistance (DR) curve for each spot weld and compare it with a previously determined optimal master data set. In case of deviations, the weld current is

Preprints (www.preprints.org) | NOT PEER-REVIEWED | Posted: 27 October 2021 doi:10.20944/preprints202110.0411.v1

controlled [8] to keep the heat input constant for all welds. The final quality documentation of the process, is carried out by the production personnel. For this purpose, destructive testing [8] is applied on random samples to measure the geometrical attributes of the weld nugget. For example, it is necessary to ensure that the weld nugget is large enough and is formed across all joining planes [9], because of its significant influence on the mechanical properties of the welded joint [10]. In this case, the quality evaluation is largely dependent on the experience of the inspector and the inspection interval [8].

A digitalized solution that provides consistent results regarding the individual quality evaluation of spot welds is desirable: Especially safety-relevant components (e.g. car bodies) require a comprehensive documentation [11] to ensure the traceability of manufacturing failures [12]. In some disciplines, e.g. additive manufacturing, there are already efforts towards the individual documentation of the component quality [13]. The aim is to evaluate the quality of an individual production step (additive manufacturing, welding, etc.) with the aid of sensors, algorithms and simulations to document it and finally to certify it [14]. Especially, the growing trend of offering highly configurable products, drives the increase of the manufacturing efforts [15]. To overcome this rise of the complexity, artificial intelligence (AI) methods are suitable tools.

As data-driven approaches, AI algorithms are appropriate to predict the RSW process [16]. They are able to model very complex, highly nonlinear relations [17]. The implementation and modelling of the algorithm represent the main effort, whereas the calculation of each weld spot can be done in real time [18]. Furthermore, AI algorithms can be used to leverage historical process data [19] in order to improve process parameter predictions. In contrast to empirical and statistical models, the AI models do not require any assumptions and prior knowledge about the physical phenomena of a context to be modelled. Commonly used AI algorithms are artificial neural networks (ANN) [20], decision trees [21] and support vector machines [20].

AI algorithms have been already used to reliably perform quality checks during manufacturing [22]. Afshari et al. [23] implemented an ANN based on process parameters to estimate the size of the weld nugget in RSW of two-sheet joints. Subsequently, the authors compared the results with a finite element simulation and found that both, ANNs and simulations are equivalent in terms of accuracy. Ahmed et al. [18] implemented a decision tree algorithm to predict the spot diameter from process parameters like: current, weld time, material and coating. The authors trained the algorithm with the whole dataset and showed that the trained parameters were sufficient to predict the nugget diameter well. Arunchai et al. [24] implemented an ANN algorithm to predict the shear strength of aluminium RSW specimens from the following parameters: current, electrode force, welding time and contact resistance. The algorithm was able to predict the shear strength accurately. The model was trained with 75% of the whole data set and tested with 25%. This so called “train-test split” technique is used to evaluate the performance of an AI algorithm. The train dataset is used to fit the model, whereas the test dataset is used to evaluate the accuracy. Panda et al. [20] implemented a support vector machine algorithm to predict the failure load of spot welded aluminium sheets. Martin et al. [25] used an ANN algorithm to evaluate the welding time, current, electrode force and to predict the tensile shear strength of spot-welding joints of AISI 304.

The accuracy and robustness of the models is dependent on the provided data for the training. Wang et al. [17] examined the application of AI models in welding for monitoring and diagnosis purposes. They acknowledged that AI algorithms can predict the observed processes well, but can have large errors when extrapolating beyond the observation range. Zhou et al. [22] stated that most AI approaches lack generality and can only be applied in limited fields where the input data is sufficiently available. Fabry et al. [26] investigated the extrapolation capabilities of an ANN model at the edge and beyond the

 doi:10.20944/preprints202110.0411.v1

trained parameter space. The authors found out, that often high deviations from the original data occurred. Therefore, they recommended to only rely on the approximation of a previously trained ANN for areas inside the parameter space of the training dataset. Hence, the evaluation of unknown data, which were not part of the training, is still challenging. A possible approach to improve the robustness is to include process signals. It can be assumed, that the behaviour of the process signals for different specimens and materials will be on average similar.

In their work, Boersch et al. [27] developed a decision tree algorithm for the prediction of weld spot diameters based on process data and features extracted from the DR curve. The authors segmented the curve and calculated for every segment different geometric and statistical features. This resulted in a highly accurate decision tree regression model to predict the weld nugget size. Wan et al. [28] used an ANN to predict the size of weld nuggets during RSW of two-sheet joints. The authors also were able to achieve a high prediction accuracy by evaluating the DR. Lee et al. [29] implemented an AI algorithm to predict the electrode misalignment based on process parameters and the DR curve. The authors showed that AI models trained with features from the DR curve are able to predict data that differs slightly from the training data.

In the literature, the authors were predicting with high accuracy target variables like nugget diameter and shear strength mainly on the basis of process data obtained from lab environments. The conditions in the industry differ from those in the laboratory. To transfer such AI models to a real manufacturing, it is necessary to prove the robustness of the models. In this paper, the weld nugget diameter will be predicted from process parameters and signals using a multi-layer perceptron (MLP) regression algorithm. Moreover, the behaviour of the AI model with a new data set, which has not been part of the training, will be tested and the extrapolation ability of the model will be investigated

2. Materials and Methods

2.1. Experimental Procedure

The welding experiments were conducted using a servo-mechanical C-type welding gun, equipped with F1-16-20-8-50-5.5 type electrode caps according to DIN EN ISO 5821 [30] and a medium frequency inverter power source. The experimental setup is illustrated in Figure 1, it includes a Rogowski-coil to measure the current and voltage sensors at the electrodes to calculate the DR for each weld. The Signals are recorded using the SPATZMulti04 Weld Checker with a maximum sampling rate of 20 kHz and an accuracy of 3% [31], which is adequate for the data acquisition in RSW [8].

The welding current range (WCR) for every steel was determined in accordance to the standard SEP 1220 [32]. The electrode force, the welding time, holding time and squeeze time were kept constant during the experiments, only the current was varied. The first weld is done with a current of 3 kA. For the further welds, the current is increased by 200 A per weld, until the first spatter occurs. Afterwards, the current is reduced by 100 A until no spatter occurs. The current at which no spatter occurs is determined as the maximum current of the WCR. The minimum current of the WCR is the current that at least creates a weld spot that is larger or equal than the minimum spot diameter, which is 4 times the square root of the sheet thickness.

After the welding experiments, destructive testing was conducted to separate the welded sheets and to measure the nugget diameter. Afterwards, the recorded process parameters and signals were linked together and saved in a database.

Preprints (www.preprints.org) | NOT PEER-REVIEWED | Posted: 27 October 2021 doi:10.20944/preprints202110.0411.v1

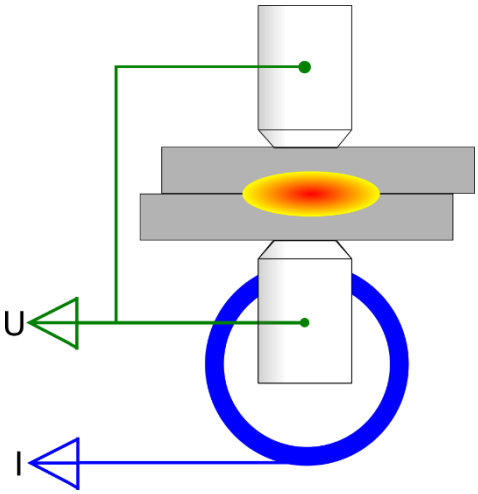

Figure 1. Experimental setup. Schematic of the welding setup: welding gun with a Rogowski coil and voltage sensors.

Figure 2.a shows an exemplary weld nugget directly after the torsion testing. In Accordance to DVS 2916-1 [33], the fracture surface after a torsion test, can be subdivided into an adhesive zone and the weld nugget. In Figure 2.b marks these areas; the blue ring denotes the adhesive zone and the yellow area the weld nugget. The weld nugget diameter is determined as the average of the vertical and horizontal measurement of extracted circle.

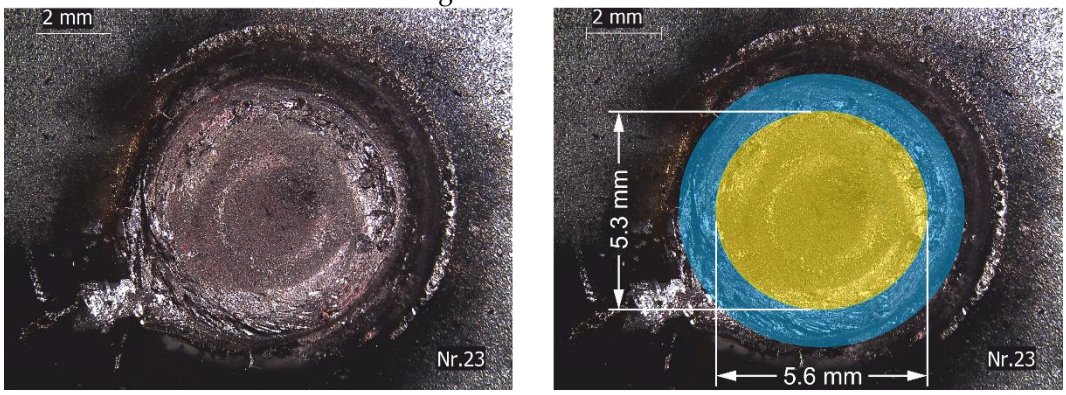

(**a**) (**b**)

Figure 2. Exemplary specimen after torsion testing: a) Weld nugget after torsion testing; b) adhesive zone is represented by the blue ring and the yellow circle marks the weld nugget.

Table 1 lists all advanced high-strength steels (AHSS), which were used in this work. The sheet thicknesses range from 1.0 mm to 2.2 mm. All the materials are of one strength class, but differ in the coating and in the specific material composition because they were provided by different suppliers.

Preprints (www.preprints.org) | NOT PEER-REVIEWED | Posted: 27 October 2021 doi:10.20944/preprints202110.0411.v1

Table 1. Material overview. Name of materials in accordance to DIN EN 10346:2015 and DIN EN 10152:2017

No.	Supplier	Name of Material	Sheet thickness
1	1	HCT 780X +ZM90	1.8
2		HCT 780X +ZE50/50	1.0
3		HCT 780X	1.5
4		HCT 780X +Z100	2.2
5		HCT 780X +Z110	1.5
6		HCT 780X +ZF100	1.5
7	2	HCT 780X +ZM120	1.5
8		HCT 780X +ZM100	1.75
9		HCT 780X +Z140	1.8

2.2. Data Analysis

The collected database consists mainly of discrete quantitative data: the applied electrode force, the current the process times, the material names and their sheet thicknesses. The DR is recorded as time-series data for each spot. All the data is linked through a weld identification number, to assure the traceability and to connect the measured diameters to the recorded data.

For pre-processing, a numeric label was assigned to each material and the data was scaled to reach similar input units. Then, the features of the DR curves were extracted. Two approaches were used in this paper. A manual feature extraction based on physical considerations was done and an automated approach using the python library "TSFRESH" [34] was applied to extract the features from the DR curves. Figure 3 shows a typical DR curve [29] with a starting point (SP), two peaks (P1 and P2) and an end point (EP). The DR curve can be subdivided into three stages. In the first stage the DR curve drops from the SP to the local minimum P1, due to current application and the enlargement of the contact surface that forces a decline of the film resistance at the faying surfaces and electrode workpiece interface. The second stage is characterized by a steep rise of the DR until it reaches the local maximum P2, due to the starting of the nugget formation and the accompanying temperature rise. With the initiating nugget solidification in the third stage, the DR curve sinks from P2 to EP until the welding process is completed. Further, the area (A) under the curve was also calculated, as it correlates with the heat input, which influences the nugget size.

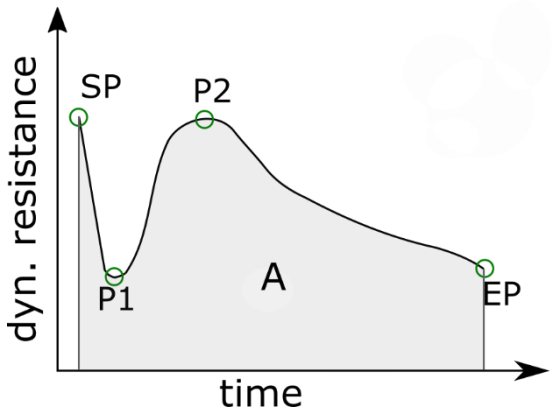

Figure 3. Typical DR curve for steel [29]. The following features are marked: Starting point (SP), Peak no. 1 (P1), Peak no. 2 (P2), end point (EP) and Area (A) under the curve.

Preprints (www.preprints.org) | NOT PEER-REVIEWED | Posted: 27 October 2021 doi:10.20944/preprints202110.0411.v1

The feature extraction tool "TSFRESH" calculated a total of 779 time-series features from the DR curve and their statistical significance. Nearly one-third of the features were labelled as statistically significant by "TSFRESH". The five most significant features were taken as input data for the AI algorithm. These features mainly include statistical values that are less descriptive than the manually extracted features from Figure 3 (e.g. the sum of reoccurring data points). However, also the global minimum of the curve was identified as one of the most significant features.

In this work, the extrapolation capabilities of the MLP model will be tested. Hence, the available data is subdivided mainly into two datasets. The first dataset includes only the data of the materials that were provided by the first supplier and the second dataset is related to the data of the materials of supplier no. 2. Then, three different models will be set up. The first model evaluates only the process parameters, the second model includes also the manual extracted features from the DR curve and the third model will be trained with the automated extracted features. All models are set up as MLP regressors with one hidden layer.

A MLP regressor is a supervised learning algorithm that learns the following function by training on a dataset:

$$f: R^m \rightarrow R^n\,, \qquad f(x) = w_{11}x_1 + w_{21}x_1 + \cdots + w_{km}x_m, \tag{1}$$

where x represents the input variables, w is devoted to the weights of the input variables, m is the number of inputs, n represents the number of outputs and k is the number of the neurons of the hidden layer.

The first model has seven input neurons with one hidden layer and one output layer. The input neurons evaluate the following parameters: current, force, base material, the base thickness, the top material and the top thickness. The second model includes the following features, which were extracted manually: starting point of the DR curve, end point, area under the curve, first and second peak and their positions on the timeline. The third model includes the five most significant features from the DR curve, which were extracted using "TSFRESH". The second and the third model have also one hidden layer and one output layer to predict the nugget size.

2.3. Evaluation Metric

The deviation between the measured diameters and the predictions will be expressed with the relative error of the prediction:

$$\delta = \frac{|\delta_p - \delta_m|}{d_m} \cdot 100\%, \tag{2}$$

with d_m as the measured nugget diameter and d_p as the prediction.

This metric will be calculated for each prediction. Then the calculated values are divided into three groups. The first group contains all predictions with an error of less than 10 %, the second group includes the predictions with an error between 10% and 20% and the last group stands for the predictions with an error larger than 20%. In this work, an error of less than 10% will be determined as a good prediction and a prediction with an error between 10% and 20% is still acceptable, whereas predictions with errors larger than 20% will be classified as an inaccurate prediction. Then, the predictions in the different groups are counted to calculate a proportion of the groups in terms of the total number of the predictions and the results will be plotted in a bar chart.

Preprints (www.preprints.org) | NOT PEER-REVIEWED | Posted: 27 October 2021 doi:10.20944/preprints202110.0411.v1

3. Results and Discussion

Figure 4 shows a scatter plot that depicts the nugget diameters over the applied current. It can be seen that the nugget size depends on the applied current. In general, an increase of the current leads to larger nugget diameters. Also, other parameters (such as electrode force, thickness and material) have an influence on the nugget formation, which can be seen in the deviations of the nuggets with the same current level. The data is subdivided into two datasets which differ mainly in the material composition and the coating of the specimens. The first dataset contains only the data related to the specimen that were made out of the materials from supplier 1 and the second dataset represents the specimen that were made out of the materials from supplier 2. Dataset 1 and 2 have some overlaps; however, they differ in the applied process parameters. For example, the weld spots of dataset 1 experienced a current from 3.2 kA to 8.3 kA, whereas the samples of dataset 2 experienced a current between 4.8 kA to 9.0 kA. In dataset 1, three different electrode forces were applied: 3.5 kN, 4.5 kN and 5.0 kN, whereas in dataset 2 only an electrode force of 4.5 kN was applied. The sheet thickness in dataset 1 ranges from 1.0 mm to 2.2 mm, whereas in dataset 2 only two sheet thicknesses were used: 1.5 mm and 1.8 mm.

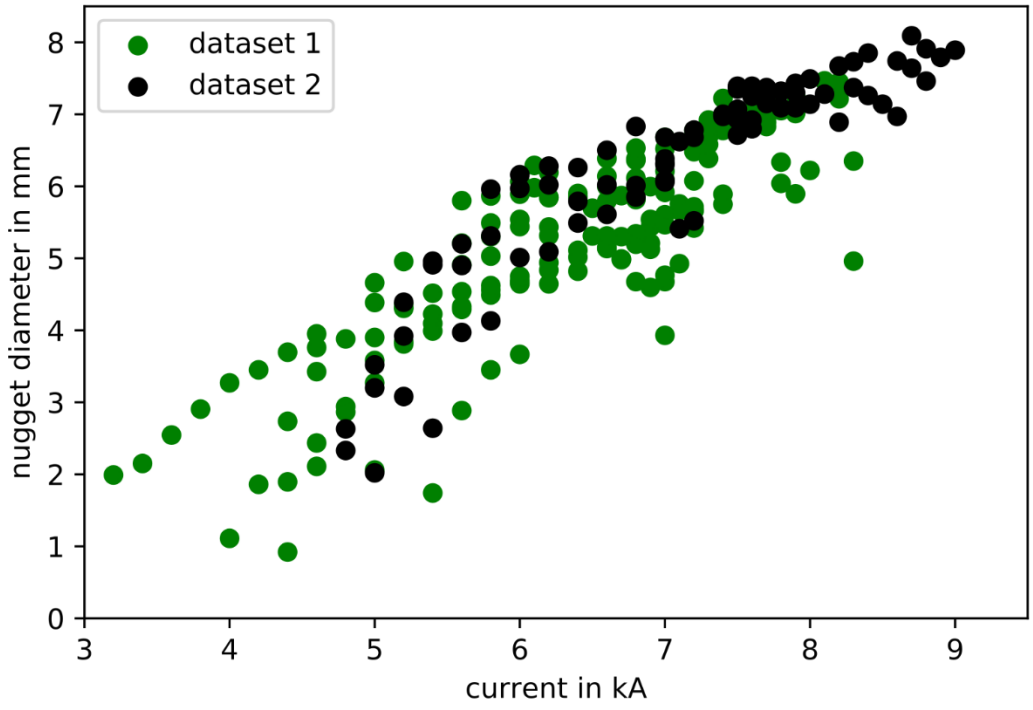

Figure 4. Data overview. Green spots marks measured diameters from supplier 1 and black spots from supplier 2.

The first MLP model was trained only with the process parameters: current, welding time, electrode force, sheet thickness and material. Figure 5.a shows a scatter plot of the measured nugget diameters from the dataset 1 and the blue crosses marks the prediction. It can be seen, that the algorithm provides a good prediction of the dataset. The bar chart shows, that 85% of the predictions had a relative deviation from the measured nugget diameters of less than 10%. Figure 5.b shows a scatter plot of the measured nugget diameters from dataset 2, which was not part of the training. Similar to the prior image, the predictions are represented by the blue crosses. It is obvious that the model overestimates the nugget diameter and it was not able to map the distribution of the nugget diameters correctly. This can also be seen in the bar chart, 90% of the predictions had a relative deviation from the real nugget diameters of more than 20%.

Preprints (www.preprints.org) | NOT PEER-REVIEWED | Posted: 27 October 2021 doi:10.20944/preprints202110.0411.v1

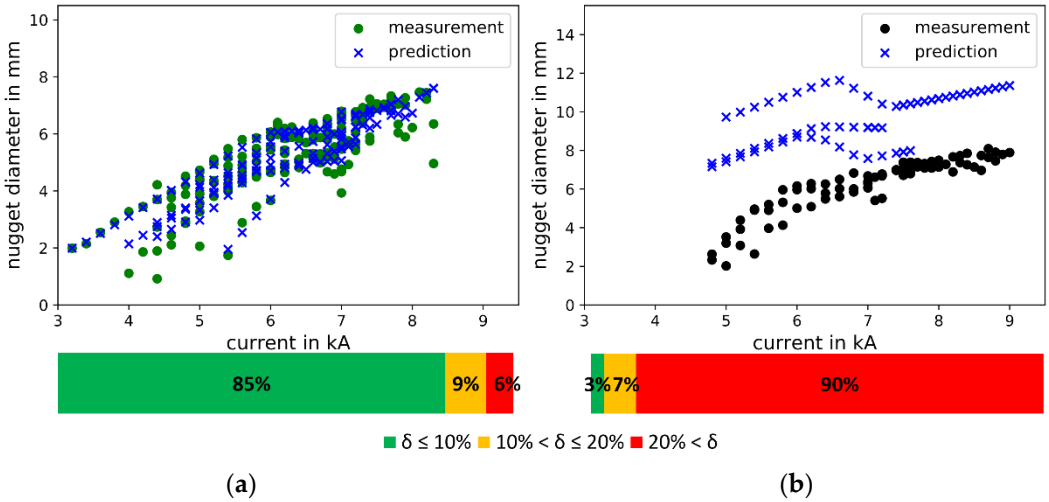

Figure 5. Predictive performance of the first model. Only process parameters were used as input for training: (**a**) scatter plot of the measured and predicted nugget diameters from dataset 1; (**b**) scatter plot of the measured and predicted nugget diameters from dataset 2. The bar charts show the predictive accuracy based on the prescribed deviation.

The second MLP model was trained with the data from dataset 1 and the manual dynamic resistance features. The features were extracted from the curves through the identification of characteristic points: SP, P1, P2, EP and A. Figure 6.a shows a scatter plot of the measured nugget diameters from dataset 1. The algorithm provides a very good prediction of the data set, similar to the first model. The bar chart shows, that 87% were predicted with an acceptable accuracy of less than 10% and the model was able to map the distribution of the nugget diameters very well. In Figure 6.b, the predictions are mostly spatially close to the measurements with a considerable number of outliers. In comparison to the first model, this model was also able to map the distribution of the nugget diameters of the untrained dataset 2. The bar chart shows that only 5% of the predictions had a relative deviation from the real nugget diameters of less than 10% and 32% have a relative deviation between 10% and 20%. The proportion of predictions with a relative error of more than 20% is still significantly smaller in this model than in the first one.

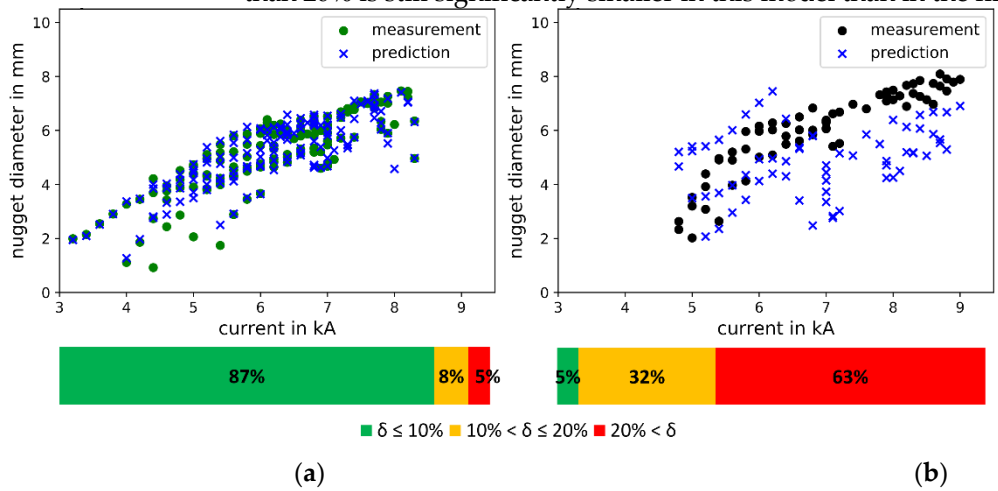

Figure 6. Predictive performance of the second model. The training included manually extracted dynamic resistance features: (**a**) scatter plot of the measured and predicted nugget diameters from dataset 1; (**b**) scatter plot of the measured and predicted nugget diameters from dataset 2. The bar charts show the predictive accuracy based on the prescribed deviation.

The third MLP model was implemented with dataset 1 and validated with dataset 2. In addition to the process parameters, the DR curves were also involved in the training. The curves were measured during the experiments and were assigned to each spot. An automated feature extraction tool "TSFRESH" was used to determine the relevant features of the DR curve. Figure 7.a shows that the third model achieved the highest accuracy rate in

Preprints (www.preprints.org) | NOT PEER-REVIEWED | Posted: 27 October 2021 doi:10.20944/preprints202110.0411.v1

predicting dataset 1. The bar chart shows, that 90% of the predictions had a relative deviation from the measured nugget diameters of less than 10%. From the scatter plot in Figure 7.b and the bar chart below it, it is obvious that the third model is the most robust algorithm in this work. The MLP regressor represents the second dataset well, which can be seen in the bar chart. 35% of the predictions had a relative deviation from the real nugget diameters of less than 10% and another 17% have a relative deviation between 10% and 20%. The proportion of predictions with a relative error of more than 20% is significantly smaller in this model than in the first and second one.

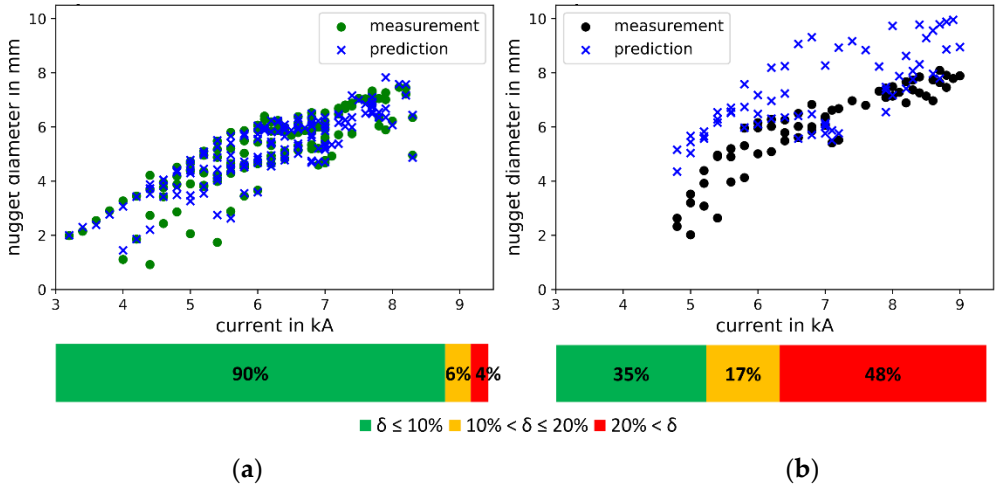

Figure 7. Predictive performance of the third model. The training included the dynamic resistance features extracted by "TSFRESH": (**a**) scatter plot of the measured and predicted nugget diameters from dataset 1; (**b**) scatter plot of the measured and predicted nugget diameters from dataset 2. The bar charts show the predictive accuracy based on the prescribed deviation.

The three models were able to predict the dataset 1 well with an accuracy ranging from 85% to 90%. From this it follows that, the structure of the models and the respective input data are sufficient to evaluate the RSW process data and to predict the weld nugget diameter. This was already shown in the literature by Afshari et al. [23]. Similar to Boersch et al. [27] and Wan et al. [28] the models 2 and 3 achieved higher accuracy rates than model 1, due to the evaluation of the dynamic resistance features.

The models were not able to achieve such high accuracy rates with dataset 2. However, the second and third model were able to yield significantly better results than the first model. Hence, the models which were trained with features from the dynamic resistance curve, can be seen as more robust than the first model that was trained only with process parameters. In contrast to the work of Fabry et al. [26], the second and third model were able to extrapolate to a certain degree. Both models leveraged the characteristic behaviour of the dynamic resistance curve [8] to predict the nugget diameter for untrained input parameters. Similar observations were made by Lee et al. [29]. The authors trained their model with calculated features based on wavelet-transformation and they succeeded in the prediction of data from outside of the trained process parameter space. In terms of predicting a dataset from outside of the parameter space of the training data, the third model performed better than the second one, because it included the most significant features of the dynamic resistance curve.

4. Conclusions

This work aimed to investigate the extrapolation capabilities of an artificial neural network algorithm to predict the nugget diameter of resistance spot welds of advanced high-strength steels. Three multi-layer perceptron models were implemented and trained on the same data set. The models predicted and mapped the trained dataset well. Hence, the process parameters and structure of the models were sufficient to represent the RSW process and to predict the nugget diameter. The first model was trained only with process parameters, whereas the second and third model were provided with features from the

dynamic resistance curve. This resulted in an increase of the predictive accuracy of both models. Two approaches were used: a manual feature picking, based on the identification of characteristic points on the dynamic resistance curve and an automated feature extraction tool that calculates a large number of possible features.
The second and third model were able to extrapolate and to predict the nugget diameters from the non-trained data set. The latter was more successful in extrapolating, because the most significant features were included. Hence, to ensure a certain level of extrapolation capability and robustness for AI algorithms in RSW, it is essential to involve process signals, like the dynamic resistance curve in the training of the AI algorithms and to choose the most significant ones for the training.

Author Contributions: Conceptualization, B.E. and M.B.; methodology, B.E.; software, B.E.; validation, B.E.; formal analysis, B.E.; investigation, B.E.; resources, M.R.; data curation, B.E.; writing—original draft preparation, B.E.; writing—review and editing, M.B and M.R..; visualization, B.E.; supervision, M.B.; project administration, B.E. All authors have read and agreed to the published version of the manuscript.

Funding: This research received no external funding. The APC was funded by Fraunhofer-Gesellschaft.

Conflicts of Interest: The authors declare no conflict of interest. The funders had no role in the design of the study; in the collection, analyses, or interpretation of data; in the writing of the manuscript, or in the decision to publish the results.

References

1. Brauser, S.; Pepke, L.A.; Weber, G.; Rethmeier, M. Deformation behaviour of spot-welded high strength steels for automotive applications. Materials Science and Engineering: A 2010, 527, 7099–7108, doi:10.1016/j.msea.2010.07.091.
2. Lei, Z.; Kang, H.; Liu, Y. Finite Element Analysis for Transient Thermal Characteristics of Resistance Spot Welding Process with Three Sheets Assemblies. Procedia Engineering 2011, 16, 622–631, doi:10.1016/j.proeng.2011.08.1133.
3. Summerville, C.; Adams, D.; Compston, P.; Doolan, M. Nugget Diameter in Resistance Spot Welding: A Comparison between a Dynamic Resistance Based Approach and Ultrasound C-scan. Procedia Engineering 2017, 183, 257–263, doi:10.1016/j.proeng.2017.04.033.
4. Nielsen, C.V.; Friis, K.S.; Bay, N. Three-Sheet Spot Welding of Advanced High-Strength Steels. Welding Journal 2011, 90, 33–40.
5. Williams, N.T.; Parker, J.D. Review of resistance spot welding of steel sheets Part 1 Modelling and control of weld nugget formation. International Materials Reviews 2004, 49, 45–75, doi:10.1179/095066004225010523.
6. Jou, M. Real time monitoring weld quality of resistance spot welding for the fabrication of sheet metal assemblies. Journal of Materials Processing Technology 2003, 132, 102–113, doi:10.1016/S0924-0136(02)00409-0.
7. Bosch Rexroth. Adapt and change: How adaptive control of resistance welding can cut production costs and improve product quality. Available online: https://m.boschrexroth.com/en/gb/trends-and-topics/adaptive-welding/seoadaptivewelding-2 (accessed on 1 April 2020).
8. Zhang, H.; Senkara, J. Resistance welding: Fundamentals and applications, 2. ed.; CRC Press: Boca Raton, Fla., 2012, ISBN 978-1-4398-5371-9.
9. Li, Y.; Yan, F.; Luo, Z.; Chao, Y.J.; Ao, S.; Cui, X. Weld Growth Mechanisms and Failure Behavior of Three-Sheet Resistance Spot Welds Made of 5052 Aluminum Alloy. J. of Materi Eng and Perform 2015, 24, 2546–2555, doi:10.1007/s11665-015-1519-9.
10. Ren, J.; Dong, W.; Zhang, Y.; Yu, Z. Failure Analysis of Three-Sheet Stackup Structure Made of Dissimilar High-Strength Steel. J. of Materi Eng and Perform 2019, 28, 3438–3445, doi:10.1007/s11665-019-04140-w.
11. HW-Verlag. Qualitätssicherung und Dokumentation Verbinden. Available online: https://werkstoffzeitschrift.de/qualitaetssicherung-und-dokumentation-verbinden/ (accessed on 13 April 2020).
12. Pereira, A.B.; Melo, F.J.M.Q. de. Quality Assessment and Process Management of Welded Joints in Metal Construction—A Review. Metals 2020, 10, 1–18, doi:10.3390/met10010115.

13. Mazumder, J. Design for Metallic Additive Manufacturing Machine with Capability for "Certify as You Build". Procedia CIRP 2015, 36, 187–192, doi:10.1016/j.procir.2015.01.009.
14. Holzmond, O.; Li, X. In situ real time defect detection of 3D printed parts. Additive Manufacturing 2017, 17, 135–142, doi:10.1016/j.addma.2017.08.003.
15. Eggink, D.H.; Groll, M.W. Joining element design and product variety in manufacturing industries. Procedia CIRP 2020, 88, 76–81, doi:10.1016/j.procir.2020.05.014.
16. Shahin, M.A. State-of-the-art review of some artificial intelligence applications in pile foundations. Geoscience Frontiers 2016, 7, 33–44, doi:10.1016/j.gsf.2014.10.002.
17. Wang, B.; Hu, S.J.; Sun, L.; Freiheit, T. Intelligent welding system technologies: State-of-the-art review and perspectives. Journal of Manufacturing Systems 2020, 56, 373–391, doi:10.1016/j.jmsy.2020.06.020.
18. Ahmed, F.; Jannat, N.-E.; Schmidt, D.; Kim, K.-Y. Data-driven cyber-physical system framework for connected resistance spot welding weldability certification. Robotics and Computer-Integrated Manufacturing 2021, 67, 102036, doi:10.1016/j.rcim.2020.102036.
19. Ashtari, E.; Semere, D.; Melander, A.; Löveborn, D.; Hedegård, J. Knowledge Platform for Resistance Spot Welding. Procedia CIRP 2018, 72, 1166–1171, doi:10.1016/j.procir.2018.03.114.
20. Panda, B.N.; Babhubalendruni, M.V.A.R.; Biswal, B.B.; Rajput, D.S. Application of Artificial Intelligence Methods to Spot Welding of Commercial Aluminum Sheets (B.S. 1050). In Proceedings of Fourth International Conference on Soft Computing for Problem Solving; Das, K.N., Deep, K., Pant, M., Bansal, J.C., Nagar, A., Eds.; Springer India: New Delhi, 2015; pp 21–32, ISBN 978-81-322-2216-3.
21. Ahmed, F.; Kim, K.-Y. Data-driven Weld Nugget Width Prediction with Decision Tree Algorithm. Procedia Manufacturing 2017, 10, 1009–1019, doi:10.1016/j.promfg.2017.07.092.
22. Zhou, K.; Yao, P. Overview of recent advances of process analysis and quality control in resistance spot welding. Mechanical Systems and Signal Processing 2019, 124, 170–198, doi:10.1016/j.ymssp.2019.01.041.
23. Afshari, D.; Sedighi, M.; Reza Karimi, M.; Barsoum, Z. Prediction of the nugget size in resistance spot welding with a combination of a finite-element analysis and an artificial neural network. Materiali in Tehnologije 2014, 48, 33–38.
24. Arunchai, T.; Sonthipermpoon, K.; Apichayakul, P.; Tamee, K. Resistance Spot Welding Optimization Based on Artificial Neural Network. International Journal of Manufacturing Engineering 2014, 2014, 1–6, doi:10.1155/2014/154784.
25. Martín, Ó.; Ahedo, V.; Santos, J.I.; Tiedra, P. de; Galán, J.M. Quality assessment of resistance spot welding joints of AISI 304 stainless steel based on elastic nets. Materials Science and Engineering: A 2016, 676, 173–181, doi:10.1016/j.msea.2016.08.112.
26. Fabry, C.; Pittner, A.; Rethmeier, M. Design of neural network arc sensor for gap width detection in automated narrow gap GMAW. Weld World 2018, 62, 819–830, doi:10.1007/s40194-018-0584-8.
27. Boersch, I.; Füssel, U.; Gresch, C.; Großmann, C.; Hoffmann, B. Data mining in resistance spot welding. Int J Adv Manuf Technol 2018, 99, 1085–1099, doi:10.1007/s00170-016-9847-y.
28. Wan, X.; Wang, Y.; Zhao, D.; Huang, Y.; Yin, Z. Weld quality monitoring research in small scale resistance spot welding by dynamic resistance and neural network. Measurement 2017, 99, 120–127, doi:10.1016/j.measurement.2016.12.010.
29. Lee, J.; Noh, I.; Jeong, S.I.; Lee, Y.; Lee, S.W. Development of Real-time Diagnosis Framework for Angular Misalignment of Robot Spot-welding System Based on Machine Learning. Procedia Manufacturing 2020, 48, 1009–1019, doi:10.1016/j.promfg.2020.05.140.
30. DIN EN ISO 5821:2010-04. Resistance welding -Spot welding electrode caps (ISO 5821:2009).
31. Matuschek Meßtechnik GmbH. SpatzMulti04 Weld Checker & Monitor for RSW. Available online: https://www.matuschek.de/weld-monitoring/multi04-weld-monitor.htm (accessed on 1 June 2021).
32. SEP-1220-2:2011-08. Prüf- und Dokumentationsrichtlinie für die Fügeeignung von Feinblechen aus Stahl: Teil 2: Widerstandspunktschweißen.
33. DVS 2916-1:2014-03. Testing of resistance welded joints - Destructive testing, quasi static.

 doi:10.20944/preprints202110.0411.v1

34. Christ, M.; Braun, N.; Neuffer, J.; Kempa-Liehr, A.W. Time Series FeatuRe Extraction on basis of Scalable Hypothesis tests (tsfresh – A Python package). Neurocomputing 2018, 307, 72–77, doi:10.1016/j.neucom.2018.03.067.